Localized Proton Motions in the Proton-Conducting Perovskites BaZr1–xScxO3Hx (x = 0.10 and 0.50) Investigated with Quasielastic

N.B. When citing this work, cite the original published paper.

(article starts on next page)

Article

Localized Proton Motions in the Proton-Conducting Perovskites BaZr$_{1-x}$Sc$_x$O$_3$H$_x$ (x = 0.10 and 0.50) Investigated with Quasielastic Neutron Scattering

Elena Naumovska, Johannes Orstadius, Adrien Perrichon, Rasmus Lavén, Michael Marek Koza,
Zach Evenson, and Maths Karlsson*

Read Online

ACCESS | ⬛ Metrics & More | 📖 Article Recommendations | 🆂🅸 Supporting Information

ABSTRACT: Acceptor-doped barium zirconates are fast proton conductors with a mechanism of proton conduction that involves proton transfers between neighboring oxide ions and rotational motions of the O−H species. Previous results from quasielastic neutron scattering (QENS) on Y-, Sc-, and In-doped BaZrO$_3$, with a dopant concentration of up to 20%, show that the QENS signal may have contributions from several different proton transfer and O−H rotational motions, which are related to different local proton environments and which occur on similar timescales and with similar activation energies, largely independent of the type and concentration of dopant atom. Here, in a combined QENS and *ab initio* molecular dynamics (AIMD) simulation study, we show that the

QENS signal of the more heavily doped material BaZr$_{1-x}$Sc$_x$O$_3$H$_x$ with x = 0.50 can be as well related to several different proton transfer and O−H rotational motions, spanning over a large range of timescales, yet with no significant differences in activation energies nor in the spatial geometry of the dynamics as compared to the systems with $x \leq 0.20$. Further, we show that accessing momentum transfers of at least 4 Å^{-1} in the QENS data is a necessity in order to extract physically meaningful jump distances for the proton transfer and the O−H rotational process, respectively.
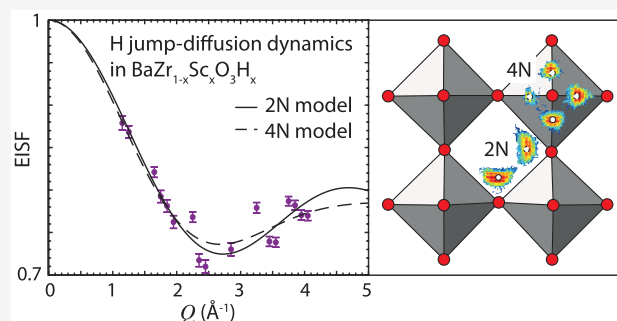
1. INTRODUCTION

Acceptor-doped perovskite oxides based on barium zirconate and barium cerate, of the general formula BaM′$_{1-x}$M″$_x$O$_{3-x/2}$ (M′ = Zr^{4+} or Ce^{4+}; M″ = trivalent cation; $0 < x < 1$), are highly attractive as proton-conducting electrolytes for various electrochemical devices.[1] The nature of proton conduction in these materials has been the subject of vast computational and experimental studies. Computationally, for instance, molecular dynamics (MD) simulations of a proton in BaCeO$_3$ showed that the proton conduction mechanism may be divided into two elementary, short-range (localized), dynamic processes, namely proton transfer between two adjacent oxygens and rotational diffusion of the proton around a specific oxygen, whereas the long-range translation of protons occurs as a series of such processes.[2] Experimentally, proton diffusion mechanisms in acceptor-doped perovskites have been mostly investigated using QENS,[3] through which both localized proton motions[4−8] and long-range proton diffusion[9,10] have been observed.

Under the reasonable assumption of four equivalent proton sites around each oxygen in a proton-conducting perovskite material, the QENS data of localized dynamics have been typically modeled as jump-diffusion dynamics over two (proton transfer) and four (rotational motion) equivalent

sites, respectively.[7,8,11,12] Although the proton transfer has been mostly identified as the rate-limiting process,[5,13−15] no consensus has been reached because it has been generally difficult to separate the contributions from proton transfer and O−H rotational diffusion in the analysis of the QENS data.[7,8] In particular, the momentum transfer (Q) range exploited in most studies (typically ∼0.2−2 Å^{-1}) has been found to be too limited to allow for a discrimination between jump-diffusion models over two and four sites, respectively. Recently, however, QENS studies of Y-, Sc-, and In-doped BaZrO$_3$, with doping levels in the range of 10−20%, have shown that such a discrimination is not solely limited by the Q range, since measurements up to ∼4 Å^{-1} showed that the quasielastic signal may be interpreted as either proton transfers or rotational motions or, actually, even to an average of such motions due to a range of different local proton sites in the materials.[7,8] With
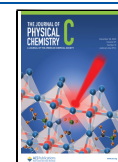
regard to more heavily doped systems, no QENS studies of localized proton dynamics have been reported so far.

In this work, we investigate the nature of localized proton dynamics in hydrated samples of Sc-doped $BaZrO_3$ with two considerably different Sc-dopant levels, i.e., 10 and 50%, using QENS together with AIMD simulations. Like in the recent QENS studies on localized proton dynamics in $BaZr_{1-x}M''_xO_{3-x/2}$ (M'' = Sc, In, and Y, and x = 0.10 and 0.20),[7,8] we exploit a large Q range up to ~4.0 Å^{-1}. In addition, we also take measurements with different energy resolutions to allow for the investigation of proton dynamics over an enlarged range of measurable timescales compared to previous works. The aim of the study is to investigate the difference in proton dynamics between the two materials and hence develop an understanding of the role of the Sc-dopant level in the mechanism of proton diffusion. Interestingly, the results reveal that the nature of localized proton dynamics is quite similar in the two materials, ultimately pointing toward a lack of correlation between doping concentration and localized proton dynamics, even in the relatively large range of dopant atom concentrations as studied here.

2. EXPERIMENT

The two samples, hydrated powders of $BaZr_{0.90}Sc_{0.10}O_{2.95}$ (10Sc/BZO) and $BaZr_{0.50}Sc_{0.50}O_{2.75}$ (50Sc/BZO), were prepared by a solid state route. Their local structural properties and hydration behavior were characterized by thermogravimetric analysis (TGA) as well as infrared (IR) and Raman spectroscopy and found to be in agreement with studies of similar proton-conducting perovskite materials; see the Supporting Information (SI). Both samples were subjected to QENS measurements on two different instruments. The samples were measured on the time-of-flight spectrometer IN6 at the Institut Laue-Langevin in Grenoble, France. The spectrometer was operated with 5.1 Å incident wavelength neutrons, yielding an energy resolution of 70 μeV at full width at half-maximum (fwhm) at the elastic line and an accessible Q range of 0.21−2.08 Å^{-1}. The powder samples were loaded into flat aluminum cans with a sample thickness of 1.5 mm. After masking out Q ranges contaminated by small-Q scattering from the sample environment and Bragg peaks of the samples, QENS spectra were obtained in the Q range of 0.57−1.90 Å^{-1} and at the temperatures T = 200, 300, 350, 400, 450, and 510 K, for both materials. The measurements at the lowest temperature, 200 K, did not show any QENS signal for any of the two materials and were used as resolution functions in the data analysis.

The very same samples were subjected to measurements on the time-of-flight spectrometer TOFTOF at the FRM II Neutron Source in Garching, Germany. TOFTOF was operated with 2.5 Å incident wavelength neutrons, yielding an energy resolution of 450 μeV at fwhm at the elastic line, and an accessible Q range at the elastic line of 0.35−4.72 Å^{-1}. After masking out Q ranges contaminated by small-Q scattering from the sample environment and Bragg peaks of the samples, QENS spectra were obtained in the Q range of 1.03−4.07 Å^{-1} and at the temperatures T = 300, 350, 400, and 450 K for both materials and, in addition, at 200 and 485 K for 50Sc/BZO and 500 K for 10Sc/BZO. A measurement of a vanadium standard at room temperature was used as a resolution function in the data analysis for 10Sc/BZO, whereas the 200 K data was used as resolution for 50Sc/BZO.

The data reduction in both experiments comprised subtraction of empty cell scattering, normalization to a vanadium standard to correct for the efficiency of different detectors, removal of bad detectors, and transformation from the scattering angle and time-of-flight domain (θ,tof) to the (Q, E) domain, where E refers to the energy transfer. The data reduction for 10Sc/BZO was performed with the LAMP software package,[16] and the data reduction for 50Sc/BZO was performed with the Mantid software.[17] The data analysis of the reduced data sets was performed within the DAVE software.[18]

The intensity of the scattered neutrons, $S(Q, E)_{meas}$, as measured in both experiments, can be expressed as

$$S(Q, E)_{meas} \propto S(Q, E) \otimes R(Q, E) + bkg(E) \qquad (1)$$

where $S(Q, E)$ is the dynamical structure factor that contains information about the dynamical properties of the respective material, $R(Q, E)$ is the instrumental resolution function, and bkg is a linearly sloping background. While, in general, $S(Q, E)$ is comprised of one coherent and one incoherent part, previous QENS studies of proton-conducting oxides, as performed under similar experimental conditions, have shown that, in a first approximation, only incoherent scattering from the protons contributes to the quasielastic signal.[3] In effect, this means that the signal can be attributed to proton self-dynamics. In our detailed analysis, $S(Q, E)$ was approximated with a function composed of one elastic component, described as the amplitude $a_D(Q)$ multiplied with a Dirac delta function $\delta(E)$, and a quasielastic component, described as the amplitude $a_L(Q)$ multiplied with a Lorentzian function $L(Q, E)$, see eq 2.

$$S(Q, E) = a_D(Q)\delta(E) + a_L(Q)L(Q, E) \qquad (2)$$

The QENS spectra, $S(Q, E)_{meas}$, were fitted over the restricted energy transfer range of $-1.7 \leq E \leq 0.7$ meV for the IN6 experiment and $-4 \leq E \leq 2$ meV for the TOFTOF experiment due to the presence of elastic scattering artifacts from the sample environment in the Stokes part of the spectra.

3. COMPUTATIONAL DETAILS

We have previously performed AIMD simulations of 12.5% Sc-doped $BaZrO_3$ (12.5Sc/BZO) and 50Sc/BZO with VASP,[19−21] using the PAW method[22,23] for the ionic core-valence interaction and semilocal PBE functional for the exchange-correlation part;[24] for details of the simulation parameters and structural models, see ref 25. The trajectories were obtained in the NVT ensemble at T = 300 K using the Nosé-Hoover thermostat.[26−28] For 4 structural models of 12.5Sc/BZO and 10 structural models of 50Sc/BZO, each featured by different starting equilibrium positions for the protons, we generated five independent 20 ps long trajectories (40 000 steps with a time step of 0.5 fs). The AIMD trajectories were integrated in time to produce nuclear density maps of the proton spatial distribution in order to identify the geometry of the localized diffusion motions already present at 300 K as well as their associated jump distances.

Note that the limited length of the trajectories is due to the difficulty in keeping the hydrogen subsystem thermalized, which is caused by the large mass difference between barium and hydrogen and the restricted size of the structural model imposed by the limitations of the AIMD technique on the number of atoms. More details on this issue are given elsewhere.[29] Due to the fragmented trajectories, only nuclear
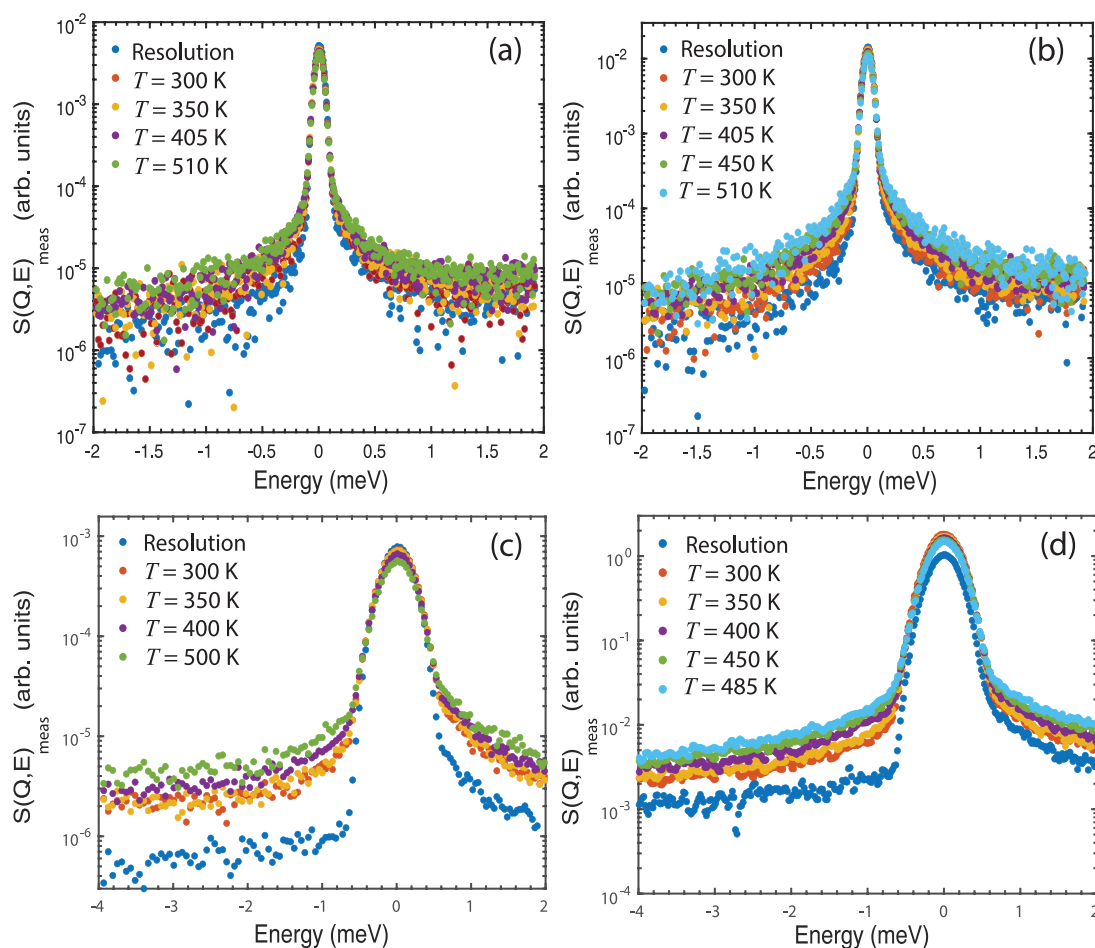
Figure 1. Temperature evolution of $S(Q,E)_{meas}$ of (a) 10Sc/BZO and (b) 50Sc/BZO summed over the Q range of 0.57−1.90 Å^{-1}, as measured on IN6, and (c) 10/BZO and (d) 50/BZO summed over the Q range of 1.03−4.07 Å^{-1}, as measured on TOFTOF.

density maps and other time-averaged quantities can be obtained. Time-dependent quantities, such as relaxation times or $S(Q, E)$ calculated from time-correlation functions, cannot be obtained.

4. RESULTS

4.1. Identification of Localized Dynamics. Figure 1 shows $S(Q, E)_{meas}$ as measured on IN6 and TOFTOF. Data are shown for both materials and for temperatures between $T =$ 300 and 500 K, together with the respective resolution functions. As can be observed, the spectra for all temperatures are characterized by a quasielastic broadening related to proton self-dynamics, and the broadening generally gets more pronounced with increasing temperature.

Figure 2 shows $S(Q, E)_{meas}$ measured on IN6 and TOFTOF, at various Q values and temperatures, together with their fits using the model of eqs 1 and 2. Note that the QENS signal is properly accounted for by a single Lorentzian function. Analysis of the fitting results showed that the fwhm (Γ) of the Lorentzian function is (within error) Q-independent (Figures S3 and S4 in the Supporting Information (SI)), for each sample and measuring temperature. This suggests that the quasielastic scattering relates to localized dynamics of the protons. This is in full accordance with our previous QENS studies on 10Sc/BZO using IN6 and IN5,[7,11] with resolutions of 100 and 620 μeV and temperature ranges of 380−495 and 200−550 K, respectively.

Depending on sample composition and temperature, the fwhm values are in the range of 0.2−0.5 meV on IN6, which corresponds to characteristic relaxation times (calculated as $2\hbar/\Gamma$) on the order of 4−8 ps for 10Sc/BZO and 5−8 ps for 50Sc/BZO. Thus, in the IN6 time window, the observed timescales of the dynamics are (within error) virtually the same in both materials. On TOFTOF, the fwhm values are in the range of 0.4−1.2 meV, which corresponds to relaxation times of the dynamics of 1.8−2.5 ps for 10Sc/BZO and 1.5−1.8 ps for 50Sc/BZO. The timescales of the dynamics are thus also comparable for the two materials in the TOFTOF time window or marginally faster in 50Sc/BZO than in 10Sc/BZO. The difference between the timescales measured on the two instruments for the same material can be rationalized by the presence of several indistinguishable localized dynamical processes due to a range of different local proton environments in the materials.

4.2. Geometry of the Localized Dynamics. To investigate the spatial geometry of the localized proton dynamics, we analyze the Q dependence of the elastic scattering intensity, here expressed as the elastic incoherent structure factor (EISF), defined as the ratio of the elastic amplitude over the sum of the elastic and quasielastic amplitudes, i.e., EISF = $a_D/(a_D + a_L)$. Note that, as previously seen in 10Sc/BZO and other related proton-conducting materials,[7,11] the QENS signal from protons experiencing motions too slow to be resolved by the instrument resolution,
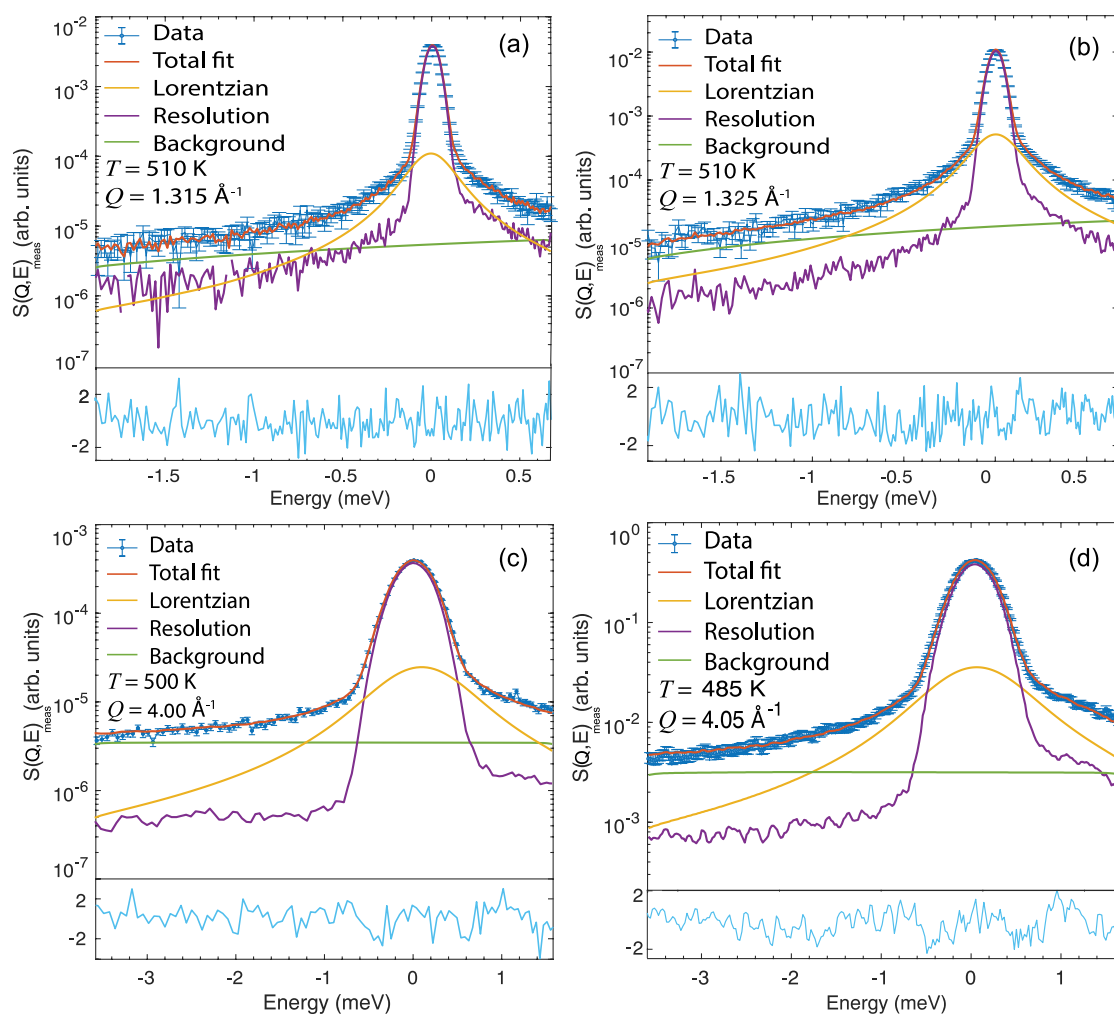
Figure 2. $S(Q, E)_{\text{meas}}$ of (a) 10Sc/BZO and (b) 50Sc/BZO at $T = 510$ K and $Q = 1.315$ Å^{-1} and $Q = 1.325$ Å^{-1}, respectively, as measured on IN6, together with fits, and (c) 10Sc/BZO and (d) 50Sc/BZO, as measured on TOFTOF at $T = 485$ K and $Q = 4.0$ Å^{-1}, together with fits. Fit residuals are indicated at the bottom of each panel.

such as long-range translational diffusion motions, will appear as additional elastic scattering. Here, in 10Sc/BZO and 50Sc/BZO, this additional elastic scattering can be interpreted as a fraction of virtually *immobile* protons.

Figure 3 shows the EISF derived from the TOFTOF data together with the Q dependencies as expected within the framework of a jump-diffusion model over two (2N) and four (4N) equivalent sites located on a circle of radius r, which can be used to describe the proton transfer and O−H rotational motion, respectively.[4] As can be seen, both models equally well describe the experimental data for all temperatures and for both materials. Note that the fitting of the EISF only gives meaningful results when considering the extended Q range of the TOFTOF data, with $Q_{\text{max}} = 4.07$ Å^{-1}. Indeed, a similar analysis on the IN6 data that are limited to $Q_{\text{max}} = 1.90$ Å^{-1} gives unphysical results (see Figure S4 and Table S1 in the SI).

The parameters obtained from the fit of the EISF derived from the TOFTOF data are listed in Table 1. Note that the jump length, d, is $d = 2 \cdot r_{2N}$ for the proton transfer, and $d = \sqrt{2} \cdot r_{4N}$ for the O−H rotation. A physically reasonable upper limit of r_{2N} (r_{2N}^{max}) can be estimated from the geometry of the high symmetry cubic structure, when considering untilted and undistorted octahedra, according to $r_{2N}^{\text{max}} = \sqrt{2}(a/2 - b)/2$. With a lattice parameter $a = 4.2$ Å

and an O−H covalent bond $b = 0.96$ Å, we obtain $r_{2N}^{\text{max}} = 0.81$ Å. The lower limit of r_{2N} is more complicated to estimate, as the jump distance of the proton transfer can vary depending on the local proton environment, the amplitude of oxygen displacement caused by the hydrogen bond, and the degree of tilt and deformation of the octahedra. Comparatively, the range of values of r_{4N} are more simple to estimate, as it should coincide with the range of O−H covalent bonds, of 0.95−1.02 Å.[5,30]

The fitted parameters in Table 1 are in the ranges of 0.75−0.79 Å for proton transfer and 0.94−1.03 Å for O−H rotational motions for 10Sc/BZO and 0.76−0.82 Å for proton transfer and 0.95−1.06 Å for O−H rotational motions for 50Sc/BZO. They are in good agreement with the results obtained in previous QENS studies on Sc-doped BaZrO$_3$. Indeed, comparable values of $r_{2N} = 0.74−0.80$ Å and $r_{4N} = 0.92−1.02$ Å were obtained from measurements of 10Sc/BZO on IN5, with a 620 μeV energy resolution and $Q_{\text{max}} = 4.6$ Å^{-1}.[7] Similarly, and despite the lower Q_{max} of 1.90 Å^{-1}, comparable values of $r_{2N} = 0.82−0.93$ Å and $r_{4N} = 0.96−1.10$ Å were obtained from measurements of 10Sc/BZO on IN6, with a 100 μeV energy resolution.[11]

The fitted values of r are thus within error identical for the two materials. However, since the fitted values of both r_{2N} and
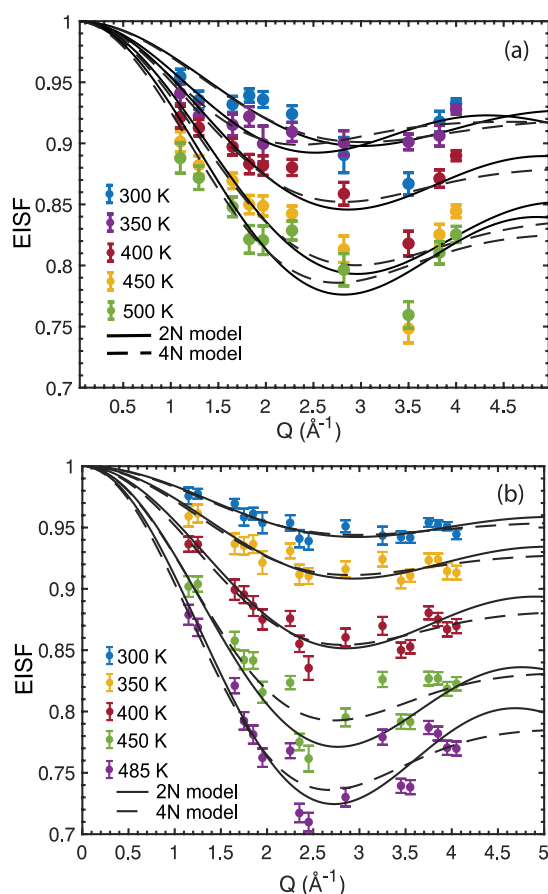
Figure 3. EISFs for (a) 10Sc/BZO and (b) 50Sc/BZO, as derived from the TOFTOF data. The lines are fits to the jump-diffusion model over two (2N) and four (4N) sites.

Table 1. Parameters from the Fits of the EISFs Derived from the TOFTOF data with Jump-Diffusion Models over Two and Four Equivalent Sites, Denoted 2N and 4N, Respectively[a]

10Sc/BZO				
T (K)	r_{2N} (Å)	c_{2N}	r_{4N} (Å)	c_{4N}
300	0.75(15)	0.830(3)	0.94(24)	0.890(2)
350	0.89(11)	0.820(2)	1.21(18)	0.880(2)
400	0.78(10)	0.740(3)	1.01(18)	0.820(2)
450	0.76(10)	0.670(4)	0.96(14)	0.770(3)
500	0.79(8)	0.630(3)	1.03(14)	0.750(2)
50Sc/BZO				
T (K)	r_{2N} (Å)	c_{2N}	r_{4N} (Å)	c_{4N}
300	0.76(5)	0.910(1)	0.95(7)	0.9400(4)
350	0.77(5)	0.850(1)	0.98(7)	0.9000(5)
400	0.78(4)	0.760(1)	1.01(6)	0.8300(7)
450	0.81(4)	0.620(2)	1.04(8)	0.760(1)
500	0.82(4)	0.540(2)	1.06(7)	0.700(1)

[a]The 350 K 10Sc/BZO fit is an outlier and is not considered further in the discussion. Numbers within parentheses represent the standard error.

r_{4N} are physically plausible, we cannot discriminate between the two models. Nonetheless, the results suggest that the localized dynamics in presence, either the proton transfer, the O—H rotation, or a mixture of both, are similar in both

materials and do not depend significantly on the Sc concentration.

Besides the parameter r related to the geometry of the localized dynamics, the parameter c is also obtained from the fit of the EISFs, which represents the fraction of immobile protons. In both materials and for both fitting models, c decreases with increasing temperature, which can be rationalized as a larger fraction of protons entering the time window of the instrument as their mobility increases with T.

Figure 4 shows the nuclear density maps calculated from the AIMD trajectories for 12.5Sc/BZO. Both proton transfer and O—H rotation motions are observed at T = 300 K in the simulations [cf. Figure 4(b,c)] although with O—H rotations in greater numbers, which suggests that the O—H rotations may be the main contributor to the QENS signal. The hydroxyl group bond lengths are found statistically identical for all protons regardless of the proximity to the Sc-dopant, with a Gaussian-shaped distribution centered at 0.990(1) Å with a standard deviation (σ) of 0.033(1) Å. Similar bond lengths are obtained for 50Sc/BZO, with a Gaussian-shaped distribution centered at 0.989(1) Å with σ = 0.033(1) Å. These values are consistent with the r_{4N} parameters of the rotational model of the O—H group obtained by QENS for both samples.

The jump distance for the proton transfer is found to be more sensitive to the proton local environments in 12.5Sc/BZO. Indeed, away from the Sc-dopant, for proton transfers not involving oxide ions marked 1 in Figure 4, the distribution of jump distances is centered at 1.608(1) Å with σ = 0.088(1) Å. This is very close to the value estimated from the geometry of the undistorted octahedra discussed earlier. Conversely, in the vicinity of the Sc-dopant, the distribution of jump distances between oxide ions marked 1 is centered at 1.132(2) Å with σ = 0.064(1) Å. This much shorter value is due mainly to the displacement of the protons toward the Sc-dopant in the asymmetric Sc—O(H)—Zr unit, as seen in Figure 4(d). Comparatively, the average proton site is located in the oxygen plane for the symmetric Zr—O(H)—Zr unit [Figure 4(e)]. Another cause for shorter proton transfer jump distances in the vicinity of Sc is the more pronounced displacement of the oxide ion under the pull of a stronger hydrogen bond. Indeed, in the vicinity of Sc, the hydrogen bond length distribution is centered at 1.903(3) Å with σ = 0.199(3) Å, while the distribution is centered at 1.950(3) Å with σ = 0.169(3) away from Sc.

A consequence of this geometrical asymmetry in the Sc—O(H)—Zr pattern is the reciprocally longer jump lengths for the proton transfer between oxide ions marked 1 and 2, which is the required process for the proton to escape the vicinity of Sc. Its jump distance distribution is centered at 1.802(1) Å with σ = 0.074(1) Å. Given the simulated jump lengths for the proton transfer, the values of r_{2N} are ~0.57 Å in the vicinity of Sc, ~0.80 Å away from it, and ~0.90 Å to escape from the vicinity of Sc. Note that the proton transfers in the vicinity of Sc, with shorter jump distances and thus lower activation energies, should be, among all proton transfer processes, the main contributor to the QENS signal. This is, however, not reflected in the experimental values of r_{2N}, in the range 0.75–0.79 Å for 10Sc/BZO, which instead correspond to proton transfers between oxide ions away from the Sc dopant. This discrepancy could indicate either that the measured QENS signal is an average of contributions from a variety of proton transfers or that, as inferred earlier, the contribution from
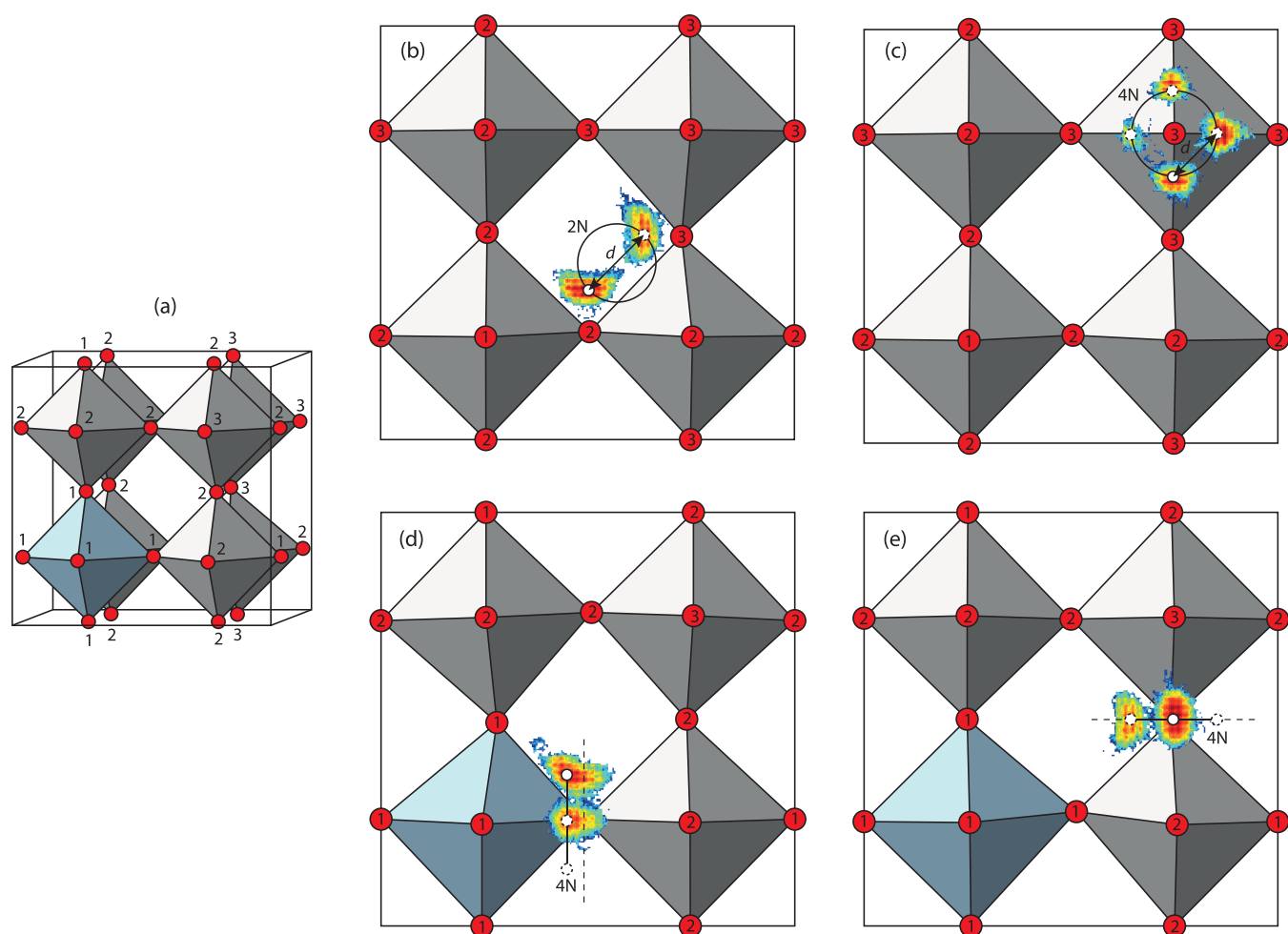
Figure 4. (a) Scheme of the 12.5Sc/BZO model. ScO_6 and ZrO_6 octahedra are represented in blue and gray, respectively. Protons and oxide ions are represented as white and red circles, respectively. Oxygen atoms are numbered from their distance to the Sc-dopant. (b−e) Nuclear density maps of the proton calculated by AIMD, together with the geometry optimized structural model, for selected trajectories.
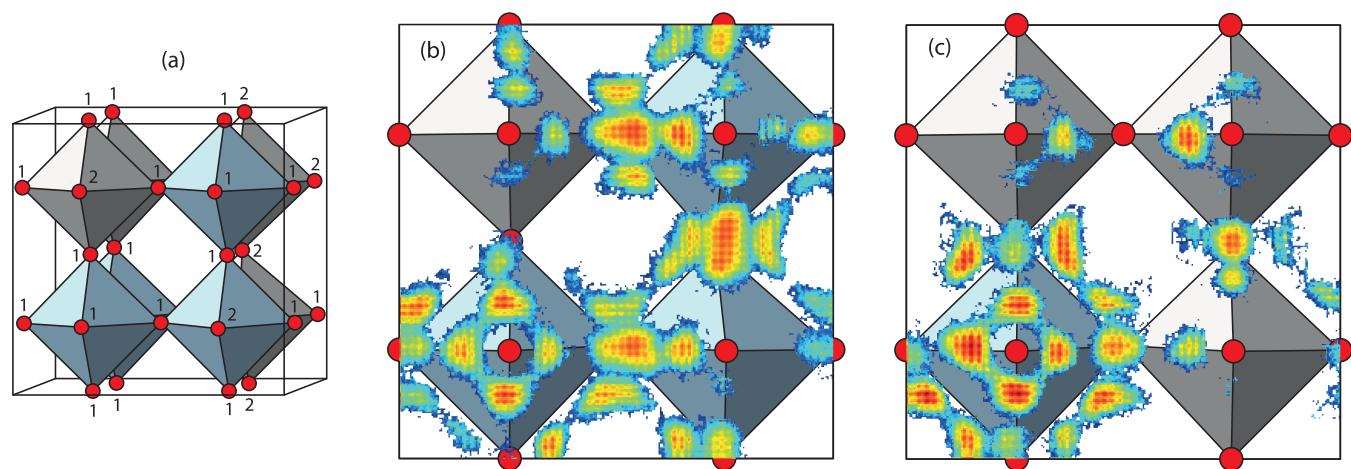

Figure 5. (a) Scheme of the 50Sc/BZO model. ScO_6 and ZrO_6 octahedra are represented in blue and gray, respectively. Oxide ions are represented as red circles. Oxygen atoms are numbered from their distance to the Sc-dopant. (b-c) Nuclear density maps of the protons calculated by AIMD using all trajectories, together with a scheme of the structural model. The nuclear densities are split between (b) the front octahedra and (c) the back octahedra, with respect to the view of (a).

proton transfers to the QENS signal is minor compared to that of the O−H rotations.

Figure 5 shows the nuclear density maps calculated from the AIMD trajectories for 50Sc/BZO. Note first that, because of the large number of Sc atoms, no oxide ions can be considered as distant (marked 3 in Figure 4, >5 Å) from Sc. Note also that out of 24 M′−O−M″ units in the simulation cell of 50Sc/BZO, there are 6 Sc−O−Sc units, 12 Sc−O−Zr units, and 6

Zr−O−Zr units. In comparison, in the 12.5Sc/BZO model, there were 6 Sc−O−Zr units and 18 Zr−O−Zr units. Finally, note that the proton nuclear densities are summed over trajectories with different initial starting positions for the four protons and thus do not reflect the relative occupation of each proton site nor the number of diffusion events. That being said, as for the simulations of 12.5Sc/BZO, we observe the presence of both proton transfers and O−H rotations in the simulations of 50Sc/BZO, with O−H rotations in greater numbers.

Interestingly, we find the proton nuclear densities to be more spatially extended in 50Sc/BZO than in 12.5Sc/BZO, which is due here to the higher degree of variability of the local proton environments. Indeed, the hydrogen bond lengths are found on average shorter in 50Sc/BZO than in 12.5Sc/BZO, with a distribution centered at 1.912(2) Å with $\sigma = 0.205(3)$ Å, which is consistent with the larger red-shift of the O−H stretch band in the IR spectrum of 50Sc/BZO [Figure S2(a)]. This implies that the amplitude of the oxide ion displacements under the effect of the hydrogen bonding network is more pronounced in 50Sc/BZO, as multiple hydrogen bonds can cooperatively contribute to stabilize more pronounced local structural distortions. This increase can be estimated from the oxide ion trajectories to ∼0.1 Å, as the maximal displacement in the plane normal to the M′−O−M″ unit is ∼0.8 Å in 50Sc/BZO and ∼0.7 Å in 12.5Sc/BZO.

Because of the increasing variety of local proton environments and more diffuse nuclear density maps, the jump distances for proton transfer are more difficult to evaluate. Nonetheless, from a selection of diffusion events, the average jump distances can be estimated to ∼1.61 Å for a proton transfer between two symmetric M′−O−M′ units and to ∼1.15 Å for a proton transfer between two asymmetric Sc−O−Zr units, with a typical standard deviation from the distribution of distances of ∼0.05 Å. These jump distances are comparable to the ones obtained for 12.5Sc/BZO. Because of the presence of adjacent Sc atoms, there is also the possibility of proton transfer from an asymmetric Zr−O−Sc unit to a symmetric Sc−O−Sc unit, which then corresponds to an average jump distance of ∼1.42 Å with $\sigma \approx 0.05$ Å. There is thus a variety of proton transfer processes with different jump lengths that can take place in the 12.5Sc/BZO and 50Sc/BZO systems.

4.3. Temperature Dependence of the Localized Dynamics. The Q averaged values of the fwhm, Γ, increase slightly with increasing temperature for both materials (Figures S3 and S4), as expected for any thermally activated process. The temperature dependence of Γ follows an Arrhenius law: $\Gamma = \Gamma_0 \exp(-E_a/k_B T)$, where Γ_0 is the trial frequency for the localized dynamics, E_a is the activation energy, and k_B is the Boltzmann constant.

Figure 6 shows the Arrhenius plot for 10Sc/BZO and 50Sc/BZO, from IN6 and TOFTOF data. Activation energies and trial frequencies obtained from the fit are reported in Table 2. While the values of E_a are, within error, similar for both materials, the activation energy of the localized diffusion dynamics in 50Sc/BZO is lower than that in 10Sc/BZO. Interestingly, slightly lower values of Γ_0 are observed in 50Sc/BZO than in 10Sc/BZO, pointing out that there is a lower attempt (trial) frequency for the proton diffusion event.

The difference in activation energies and trial frequencies between the IN6 and TOFTOF data for the same material is rationalized, in a similar way than previously discussed for the timescales, by differences in the distribution of distinct proton environment contributions given the resolution of the two
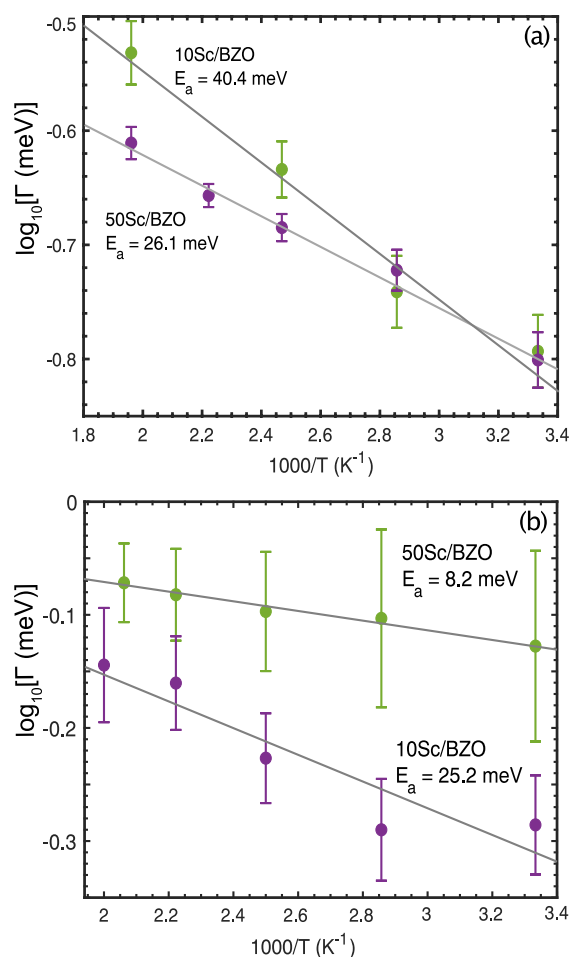

Figure 6. Temperature dependence of the Q averaged quasielastic width Γ for (a) 10Sc/BZO and 50Sc/BZO, as determined from the IN6 data, and (b) 10Sc/BZO and 50Sc/BZO, as determined from the TOFTOF data.

Table 2. Parameters from the Fits of the Temperature Dependence of the FWHMs by an Arrhenius Law[a]

Instrument	Sample	E_a (meV)	Γ_0 (meV)
IN6	10Sc/BZO	40(16)	0.7(3)
	50Sc/BZO	26(18)	0.4(1)
TOFTOF	10Sc/BZO	25(17)	1.3(4)
	50Sc/BZO	8(3)	1.1(1)

[a]Numbers within parentheses represent the standard error.

instruments. It follows that the proton environments with relatively faster timescales that contribute to the TOFTOF data also exhibit relatively higher trial frequencies and lower activation energies than the proton environments with relatively slower timescales contributing to the IN6 data.

The obtained activation energies in the range of 8−40 meV are in good agreement with the values found for localized proton dynamics in previous QENS studies of acceptor-doped $BaZrO_3$ materials, which are in the range of 10−30 meV.[5,11,31] The activation energies are also consistent with the results of the AIMD simulations. Indeed, while we cannot extract activation energies for specific localized processes from the simulations, the presence of O−H rotations and proton transfers with various jump lengths, already at 300 K, suggests

that their activation energies are on the order of 25 meV or lower.

5. DISCUSSION

As demonstrated in the EISF analysis of the TOFTOF and IN6 QENS data, accessing an extended Q range up to ~ 4 Å^{-1}, in order to resolve the minima of the EISF around $2.5-3$ Å^{-1}, is necessary to obtain physically reasonable values for the jump distances for the proton transfer and O−H rotation motions. The geometrical parameter r of the fit with the 2N and 4N jump-diffusion models that describe the proton transfer and O−H rotation motions, respectively, takes values of $r_{2N} = 0.75-0.82$ Å and $r_{4N} = 0.94-1.06$ Å for both materials. These values are in good agreement with other experimental and theoretical studies.[5,11,31,32] As per the AIMD simulations and previous studies by density functional theory calculations on BaZr$_{0.875}$Sc$_{0.125}$O$_{2.937}$ and related proton-conducting perovskites,[11,25,33,34] the proton transfer jump length between asymmetric M′−O−M″ units (here Sc−O−Zr) is expected to be significantly shorter than between symmetric M′−O−M′ units. For instance, previous DFT calculations on 3.7Sc/BZO determined a jump distance of 0.89 Å for jumps from symmetrical sites of the type Zr−O−Zr, 0.72 Å for jumps from asymmetrical sites of the type Zr−O−Sc, and 0.82 Å for jumps from (symmetrical) sites far from any dopant atom.[11] In our AIMD simulations, the jump distances for proton transfers involving an asymmetric unit are found in the range of $1.13-1.42$ Å, compared to ~ 1.6 Å between symmetric units, which is in agreement with O−O distances between 2.6 and 2.9 Å and O−H bonds between 0.97 and 1.0 Å as determined by diffraction experiments and computer simulations.[7,30,35−37]

Given the presence of proton transfers and O−H rotations in the AIMD already at 300 K, and since both 2N and 4N jump-diffusion fitting models give physically reasonable jump distances in the EISF analysis, we cannot uniquely assign the QENS signal to a specific proton transfer or O−H rotation motion. Instead, it is likely that the QENS signal originates from an average of several contributions from proton transfers with various jump distances as well as O−H rotations. On a similar note, the activation energies, quasielastic widths, and mean residence times most likely represent an average of the several contributions and hence do not represent activation energies for a specific process but rather an average of the probed contributions. This is in agreement with our previous QENS studies on the relatively weakly doped materials 10M/BZO (M = Sc, Y, and In) and 20In/BZO, which showed that the QENS signal could be ascribed to the combined contribution from several proton transfer and O−H rotation motions, associated with different local proton coordination environments, as an effect of the locally disordered nature of the structure due to the acceptor-doping of these materials.[7,8] In accordance with these studies, the present QENS results suggest that this also applies to the more heavily doped material 50Sc/BZO. It follows that the nature of the localized proton dynamics does not appear to be significantly affected by the dopant concentration within the relatively large range of dopant concentrations, 10−50%, as investigated here.

On average, faster timescales and lower activation energies are observed for 50Sc/BZO than for 10Sc/BZO, with also a slightly larger fraction of mobile protons freed at higher temperatures and decreased trial frequency. The lower activation energy could be related to the increase in the proportion of asymmetric units from 20% in 10Sc/BZO,

assuming that the Sc dopants are dispersed in the Zr matrix, to 50% in 50Sc/BZO, assuming a random distribution of Zr and Sc on the M′-site. Consequently, we expect a relatively higher population of proton transfers with shorter jump distances in 50/ScBZO than in 10Sc/BZO. As the activation energy for the proton transfer is correlated to the jump length, a shorter proton transfer jump length, averaged over all proton transfers contributing in the time window of the instrument, could explain the lower activation energies found in 50Sc/BZO than in 10Sc/BZO.

Furthermore, note that in the temperature range studied here, the proton dynamics are discussed as phonon-mediated,[38] where the collective dynamics of the host perovskite lattice help promote proton diffusion events. In this context, we speculate that the lower activation energies and trial frequencies in 50Sc/BZO than in 10Sc/BZO could as well originate from a modification of the lattice dynamics, with, for instance, a frequency shift of phonons involved in the proton transfer process toward lower energy or the presence of additional localized oxygen modes. This would be consistent with experimental observations by Raman scattering, in the lattice dynamics region of the spectra, of broader bands as well as additional bands in 50Sc/BZO with respect to 10Sc/BZO,[25] see also Figure S2(b). This would also be consistent with the increased displacement amplitude of the oxygen atoms and increased variety of proton local environments with stronger hydrogen bonding observed in the AIMD.

6. CONCLUSIONS

To conclude, we have investigated the nature of localized proton motions in the two perovskite-type proton conductors BaZr$_{1-x}$Sc$_x$O$_{3-x/2}$ with $x = 0.10$ and $x = 0.50$, using QENS together with AIMD simulations. The results reveal the presence of localized proton motions characterized by residence times on the order of a few picoseconds and an apparent activation energy of a few tens of meV, with no clear difference in proton dynamics between the two materials. In accordance with previous QENS studies of relatively weakly doped systems under similar experimental conditions, analysis of the QENS data suggests that the localized dynamics contributing to the QENS signal contains footprints of several different proton transfer and rotational motions related to different local proton configurations in the material. Note that, while the discrimination between proton transfer and O−H rotational processes in the QENS data is not possible for the present system, accessing momentum transfers as large as 4 Å^{-1} is required to extract physically meaningful jump distances.

■ ASSOCIATED CONTENT

ⓢ Supporting Information

The Supporting Information is available free of charge at https://pubs.acs.org/doi/10.1021/acs.jpcc.3c06138.

     Thermal gravimetric data for all samples; IR and Raman spectra for all samples; QENS fitting results; EISF fitting results; description of jump-diffusion models (PDF)

■ AUTHOR INFORMATION

Corresponding Author

     Maths Karlsson − *Department of Chemistry and Chemical Engineering, Chalmers University of Technology, SE-412 96 Göteborg, Sweden;* ⓞ orcid.org/0000-0002-2914-6332; Email: maths.karlsson@chalmers.se

Authors

Elena Naumovska − *Department of Chemistry and Chemical Engineering, Chalmers University of Technology, SE-412 96 Göteborg, Sweden;* ⊙ orcid.org/0000-0001-6011-5369

Johannes Orstadius − *Department of Chemistry and Chemical Engineering, Chalmers University of Technology, SE-412 96 Göteborg, Sweden*

Adrien Perrichon − *ISIS Facility, Rutherford Appleton Laboratory, Chilton, Didcot, Oxfordshire OX11 0QX, United Kingdom;* ⊙ orcid.org/0000-0003-0520-0469

Rasmus Lavén − *Department of Chemistry and Chemical Engineering, Chalmers University of Technology, SE-412 96 Göteborg, Sweden*

Michael Marek Koza − *Institut Laue-Langevin, 38042 Grenoble Cedex 9, France*

Zach Evenson − *Heinz Maier-Leibnitz Zentrum (MLZ) and Physik Department, Technische Universität München, Garching 85748, Germany*

Complete contact information is available at:
https://pubs.acs.org/10.1021/acs.jpcc.3c06138

Notes

The authors declare no competing financial interest.

■ REFERENCES

(1) Coduri, M.; Karlsson, M.; Malavasi, L. Structure−property correlation in oxide-ion and proton conductors for clean energy applications: recent experimental and computational advancements. *J. Mater. Chem. A* **2022**, *10*, 5082−5110.

(2) Münch, W.; Seifert, G.; Kreuer, K. D.; Maier, J. A quantum molecular dynamics study of proton conduction phenomena in BaCeO$_3$. *Solid State Ionics* **1996**, *86−88*, 647−652.

(3) Karlsson, M. Proton dynamics in oxides: insight into the mechanics of proton conduction from quasielastic neutron scattering. *Phys. Chem. Chem. Phys.* **2015**, *17*, 26−38.

(4) Hempehnann, R.; Karmonik, C.; Matzke, T.; Cappadonia, M.; Stimming, U.; Springer, T.; Adams, M. A. Quasielastic neutron scattering study of proton diffusion in SrCe$_{0.95}$Yb$_{0.05}$H$_{0.02}$O$_{2.985}$. *Solid State Ionics* **1995**, *77*, 152−156.

(5) Matzke, T.; Stimming, U.; Karmonik, C.; Soetratmo, M.; Hempelmann, R.; Güthoff, F. Quasielastic thermal neutron scattering experiment on the proton conductor SrCe$_{0.95}$Yb$_{0.05}$H$_{0.02}$O$_{2.985}$. *Solid State Ionics* **1996**, *86−88*, 621−628.

(6) Karmonik, C.; Hempelmann, R.; Cook, J.; Güthoff, F. Investigation of the proton migration mechanism in the perovskite proton conductor Ba$_3$Ca$_{1.18}$Nb$_{1.82}$H$_{0.2}$O$_{8.83}$ by means of quasielastic neutron scattering. *Ionics* **1996**, *2*, 69.

(7) Noferini, D.; Koza, M. M.; Karlsson, M. Localized proton motions in acceptor-doped barium zirconates. *J. Phys. Chem. C* **2017**, *121*, 7088−7093.

(8) Noferini, D.; Koza, M. M.; Rahman, S. M. H.; Evenson, Z.; Nilsen, G. J.; Eriksson, S.; Wildes, A. R.; Karlsson, M. Role of the doping level in localized proton motions in acceptor-doped barium zirconate proton conductors. *Phys. Chem. Chem. Phys.* **2018**, *20*, 13697−13704.

(9) Pionke, M.; Mono, T.; Schweika, W.; Springer, T.; Schober, H. Investigation of the hydrogen mobility in a mixed perovskite: Ba[Ca$_{(1+x)/3}$Nb$_{(2−x)/3}$]O$_{3−x/2}$ by quasielastic neutron scattering. *Solid State Ionics* **1997**, *97*, 497−504.

(10) Karlsson, M.; Engberg, D.; Björketun, M. E.; Matic, A.; Wahnström, G.; Sundell, P. G.; Berastegui, P.; Ahmed, I.; Falus, P.; Farago, B.; et al. Using neutron spin-echo to investigate proton dynamics in proton-conducting perovskites. *Chem. Mater.* **2010**, *22*, 740−742.

(11) Karlsson, M.; Matic, A.; Engberg, D.; Björketun, M. E.; Koza, M. M.; Ahmed, I.; Wahnström, G.; Börjesson, L.; Eriksson, S. G. Quasielastic neutron scattering of hydrated BaZr$_{0.90}$A$_{0.10}$O$_{2.95}$ (A= Y and Sc). *Solid State Ionics* **2009**, *180*, 22.

(12) Noferini, D.; Koza, M. M.; Fouquet, P.; Nilsen, G. J.; Kemei, M. C.; Rahman, S. M. H.; Maccarini, M.; Eriksson, S.; Karlsson, M. Proton Dynamics in Hydrated BaZr$_{0.90}$A$_{0.10}$O$_{2.95}$ (M = Y and Sc) Investigated with Neutron Spin-Echo. *J. Phys. Chem. C* **2016**, *120*, 13963−13969.

(13) Kim, D.-H.; Kim, B.-K.; Kim, Y.-C. Energy barriers for proton migration in yttrium-doped barium zirconate super cell with Σ5(310)/[001] tilt grain boundary. *Solid State Ionics.* **2012**, *213*, 18−21.

(14) Gomez, M. A.; Griffin, M. A.; Jindal, S.; Rule, K. D.; Cooper, V. R. The effect of octahedral tilting on proton binding sites and transition states in pseudo-cubic perovskite oxides. *J. Chem. Phys.* **2005**, *123*, 094703.

(15) Karlsson, M.; Björketun, M. E.; Sundell, P. G.; Matic, A.; Wahnström, G.; Engberg, D.; Börjesson, L.; Ahmed, I.; Eriksson, S. G.; Berastegui, P. Vibrational properties of protons in hydrated BaIn$_x$Zr$_{1−x}$O$_{3−x/2}$. *Phys. Rev. B* **2005**, *72*, 094303.

(16) Richard, D.; Ferrand, M.; Kearley, G. J. Analysis and visualisation of neutron-scattering data. *J. Neutron Res.* **1996**, *4*, 33−39.

(17) Arnold, O.; Bilheux, J.; Borreguero, J.; Buts, A.; Campbell, S.; Chapon, L.; Doucet, M.; Draper, N.; Ferraz Leal, R.; Gigg, M.; et al. Mantid—Data analysis and visualization package for neutron scattering and μ SR experiments. *Nucl. Instrum. Methods Phys. Res., Sect. A* **2014**, *764*, 156−166.

(18) Azuah, R.; Kneller, L.; Qiu, Y.; Tregenna-Piggott, P. L. W.; Brown, C.; Copley, J.; Dimeo, R. DAVE: a comprehensive software suite for the reduction, visualization, and analysis of low energy neutron spectroscopic data. *J. Res. Natl. Inst. Stand. Technol.* **2009**, *114*, 341−358.

(19) Kresse, G.; Hafner, J. *Ab initio* molecular dynamics for open-shell transitions metals. *Phys. Rev. B* **1993**, *48*, 13115.

(20) Kresse, G.; Hafner, J. *Ab initio* molecular dynamics for open-shell transition metals. *Phys. Rev. B* **1994**, *49*, 14251−14269.

(21) Kresse, G.; Furthmüller, J. Efficient iterative schemes for *ab initio* total-energy calculations using a plane-wave basis set. *Phys. Rev. B* **1996**, *54*, 11169.

(22) Blöchl, P. E. Projector augmented-wave method. *Phys. Rev. B* **1994**, *50*, 17953.

(23) Kresse, G.; Joubert, D. From ultrasoft pseudopotentials to the projector augmented-wave method. *Phys. Rev. B* **1999**, *59*, 1758−1775.

(24) Perdew, J. P.; Burke, K.; Ernzerhof, M. Generalized gradient approximation made simple. *Phys. Rev. Lett.* **1996**, *77*, 3865−3868.

(25) Mazzei, L.; Perrichon, A.; Mancini, A.; Malavasi, L.; Parker, S. F.; Börjesson, L.; Karlsson, M. Local coordination of protons in In- and Sc-doped BaZrO$_3$. *J. Phys. Chem. C* **2019**, *123*, 26065−26072.

(26) Bylander, D. M.; Kleinman, L. Energy fluctuations induced by the Nosé thermostat. *Phys. Rev. B* **1992**, *46*, 13756−13761.

(27) Nosé, S. A unified formulation of the constant temperature molecular dynamics methods. *J. Chem. Phys.* **1984**, *81*, 511−519.

(28) Nosé, S. Constant Temperature Molecular Dynamics Methods. *Prog. Theor. Phys. Suppl.* **1991**, *103*, 1−46.

(29) Perrichon, A.; Koza, M. M.; Evenson, Z.; Frick, B.; Demmel, F.; Fouquet, P.; Karlsson, M. Proton Diffusion Mechanism in Hydrated Barium Indate Oxides. *Chem. Mater.* **2023**, *35*, 6713−6725.

(30) Zeudmi Sahraoui, D.; Mineva, T. Effect of dopant nature on structures and lattice dynamics of proton-conducting BaZrO$_3$. *Solid State Ionics* **2013**, *253*, 195−200.

(31) Noferini, D.; Koza, M. M.; Rahman, S. M. H.; Evenson, Z.; Nilsen, G. J.; Eriksson, S.; Wildes, A. R.; Karlsson, M. Role of the doping level in localized proton motions in acceptor-doped barium zirconate proton conductors. *Phys. Chem. Chem. Phys.* **2018**, *20*, 13697−13704.

(32) Kreuer, K. D.; Fuchs, A.; Maier, J. HD isotope effect of proton conductivity and proton conduction mechanism in oxides. *Solid State Ionics* **1995**, *77*, 157−162.

(33) Björketun, M. E.; Sundell, P. G.; Wahnström, G. Structure and thermodynamic stability of hydrogen interstitials in BaZrO$_3$ perovskite oxide from density functional calculations. *Faraday Discuss.* **2007**, *134*, 247−265.

(34) Mazzei, L.; Perrichon, A.; Mancini, A.; Wahnström, G.; Malavasi, L.; Parker, S. F.; Börjesson, L.; Karlsson, M. Local structure and vibrational dynamics in indium-doped barium zirconate. *J. Mater. Chem. A* **2019**, *7*, 7360−7372.

(35) Giannici, F.; Longo, A.; Kreuer, K.-D.; Balerna, A.; Martorana, A. Dopants and defects: Local structure and dynamics in barium cerates and zirconates. *Solid State Ionics* **2010**, *181*, 122−125.

(36) Ahmed, I.; Karlsson, M.; Eriksson, S.-G.; Ahlberg, E.; Knee, C. S.; Larsson, K.; Azad, A. K.; Matic, A.; Börjesson, L. Crystal structure and proton conductivity of BaZr$_{0.9}$Sc$_{0.1}$O$_{3-\delta}$. *J. Am. Chem. Soc.* **2008**, *91*, 3039−3044.

(37) Giannici, F.; Shirpour, M.; Longo, A.; Martorana, A.; Merkle, R.; Maier, J. Long-range and short-range structure of proton-conducting Y:BaZrO$_3$. *Chem. Mater.* **2011**, *23*, 2994−3002.

(38) Braun, A.; Duval, S.; Ried, P.; Embs, J.; Juranyi, F.; Strässle, T.; Stimming, U.; Hempelmann, R.; Holtappels, P.; Graule, T. Proton diffusivity in the BaZr$_{0.9}$Y$_{0.1}$O$_{3-\delta}$ proton conductor. *J. Appl. Electrochem.* **2009**, *39*, 471−475.

(39) Karlsson, M.; Fouquet, P.; Frick, B.; Koza, M. M.; Orstadius, J.; Österberg, C.; Perrichon, A.; Wahnström, G. *Nature of hydride-ion mobility in peculiar perovskite oxyhydrides*. Institut Laue−Langevin, 2014. DOI: 10.5291/ILL-DATA.7-03-137.